OPEN ACCESS

# Unveiling the Impact of Solvent Fluorination on Ether-Based Electrolytes in Sodium-Ion Pouch Cells

*Journal of The Electrochemical Society*, 2025 **172** 110535

# Unveiling the Impact of Solvent Fluorination on Ether-Based Electrolytes in Sodium-Ion Pouch Cells

**Rishivandhiga Jayakumar,[1,2] Benjamin Cousineau,[3] Vincent L. Chevrier,[3] Chanmonirath (Michael) Chak,[1,2,4] Vadim Shipitsyn,[1,2,4] Allen Zheng,[5] Yuwei Zhu,[6] Glenn Pastel,[7,z] Zhiao Yu,[8] Linqin Mu,[6] Steve G. Greenbaum,[5] and Lin Ma[1,2,4,*,z]**

[1]*Department of Mechanical Engineering and Engineering Science, The University of North Carolina at Charlotte, Charlotte, North Carolina 28223, United States of America*
[2]*Battery Complexity, Autonomous Vehicle and Electrification (BATT CAVE) Research Center, The University of North Carolina at Charlotte, Charlotte, North Carolina 28223, United States of America*
[3]*Cyclikal LLC, St. Paul, Minnesota 55114, United States of America*
[4]*Department of Applied Physical Sciences, The University of North Carolina at Chapel Hill, Chapel Hill, North Carolina 27514, United States of America*
[5]*Department of Physics, Hunter College, City University of New York, New York, United States of America*
[6]*Materials Science and Engineering, School of Engineering for Matter, Transport, and Energy, Arizona State University, Tempe, Arizona 85281, United States of America*
[7]*Battery Sciences Branch, DEVCOM Army Research Laboratory, Adelphi, Maryland 20783, United States of America*
[8]*Feon Energy Inc., Woburn, Massachusetts 01801, United States of America*

Sodium-ion batteries (SIBs) with Earth-abundant elements are promising for global electrification, but electrolyte stability impacts electrochemical performance and safety. This study compares non-fluorinated 1,2-diethoxyethane (DEE) and fluorinated 1,2-bis(2,2-difluoroethoxy)ethane (F4DEE) as electrolyte solvents in $Na_{0.97}Ca_{0.03}[Mn_{0.39}Fe_{0.31}Ni_{0.22}Zn_{0.08}]O_2$ (NCMFNZO)/hard carbon (HC) pouch cells up to 4.0 V. Fluorination slightly reduces ionic conductivity and increases viscosity but significantly enhances electrochemical stability and safety. Cells with F4DEE exhibit lower impedance, reduced gas evolution, and less voltage decay during high-voltage storage at 40 °C. Long-term cycling shows 85% capacity retention after 500 cycles at 25 °C and 80% at 40 °C with less transition metal dissolution, outperforming DEE-based cells. Isothermal microcalorimetry reveals lower parasitic heat generation with F4DEE, while soft X-ray absorption spectroscopy confirms stabilized Ni and Mn oxidation states, indicating suppressed electrolyte oxidation. Accelerating rate calorimetry reveals improved thermal stability with F4DEE. These findings highlight fluorinated ether solvents as a promising approach to enhance SIB lifespan and safety, with ongoing challenges requiring further solvent and additive optimization.

 [DOI: 10.1149/1945-7111/ae204f]

Manuscript submitted September 12, 2025; revised manuscript received October 15, 2025. Published November 25, 2025.

Supplementary material for this article is available online

The development of sodium-ion battery (SIB) technology with long lifetimes and robust safety has gained renewed attention as global electrification expands and complementary energy-storage chemistries to lithium-ion systems are sought.[1,2] SIBs offer cost and resource-availability advantages for large-scale applications, but realizing competitive lifetime and safety requires improvements across all the cell parts including cathode, anode, electrolyte, and separator.[3,4]

Among these cell components, the electrolyte plays a central role in determining the electrochemical performance because it governs ion transport, desolvation kinetics, and formation/evolution of electrode–electrolyte interphases (EEI).[5,6] While ester-based electrolytes remain the most widely used in commercial SIB research, ether-based solvents have attracted interest because of their weaker solvation binding to $Na^+$, which enables faster desolvation and improved kinetics. In addition, ethers typically possess a higher lowest unoccupied molecular orbital (LUMO) energy level than many esters, which makes them intrinsically more resistant to reductive decomposition and thus attractive for low-voltage anodes, especially hard-carbon (HC).[7,8] However, a major drawback of conventional ethers is their susceptibility to oxidative decomposition at high cathode potentials, leading to parasitic reactions, gas generation, cathode–electrolyte interphase (CEI) degradation, and ultimately shortened cell life and safety risks.[8,9]

Fluorination of ether solvents has emerged as an effective strategy to mitigate high-voltage oxidation and to improve chemical and thermal stability, and its benefits have been widely demonstrated in lithium-ion batteries.[10,11] Hizbullin et al.[12] introduced 2,2-difluoro-1,3-dimethoxypropane (FDMPr), a novel fluorinated ether that enabled $LiNi_{0.8}Mn_{0.1}Co_{0.1}$/Li cells to retain 80% of discharge capacity after 520 cycles. Zhang and Xue et al.[13,14] reported the mono-fluorinated linear ether bis(2-fluoroethoxy)methane (BFME), which forms a LiF-rich CEI and improved $LiFePO_4$/graphite cell lifetimes across a wide temperature range, delivering 83.2%, 92.5%, and 81.2% capacity retention after 1250, 200, and 300 cycles at 25 °C, −20 °C, and 60 °C, respectively. Zhao et al.[15] introduced 1,1,1-trifluoro-2,3-dimethoxypropane (TFDMP), which afforded oxidation stability up to 4.8 V, suppressed Al corrosion, and yielded 81% retention after 200 cycles at 0.1 A $g^{-1}$. Despite these successes in Li-based systems, reports of fluorinated ethers for SIBs remain limited, and direct head-to-head comparisons between fluorinated and non-fluorinated ethers, particularly in pouch-cell formats, are largely absent.

In this work, we systematically evaluate the effects of solvent fluorination in 210 mAh $Na_{0.97}Ca_{0.03}[Mn_{0.39}Fe_{0.31}Ni_{0.22}Zn_{0.08}]O_2$ (NCMFNZO)/HC pouch cells by comparing non-fluorinated diethyl ether (DEE) and a fluorinated analogue (i.e. 1,2-bis(2,2-difluoroethoxy)ethane (F4DEE)) as the primary electrolyte solvent. While fluorination modestly reduced bulk transport properties, F4DEE maintained adequate $Na^+$ transport to support full-cell operation. After formation, F4DEE-containing cells exhibited lower impedance on the HC anode, and during high-temperature storage showed smaller voltage drop, reduced gas evolution, and less impedance growth at both cathode and anode. Long-term cycling reaffirmed the superiority of F4DEE-containing cells by achieving 85% capacity retention after 500 cycles at 25 °C and 80% at 40 °C with less transition metal dissolution. Isothermal microcalorimetry revealed

*Electrochemical Society Member.
[z]E-mail: glenn.r.pastel.civ@army.mil; l.ma@unc.edu

lower parasitic reaction heat generation in F4DEE containing cells, particularly from electrolyte oxidation. Soft X-ray absorption spectroscopy (XAS) of the CEI indicated preserved Ni and Mn oxidation states with F4DEE, further confirming electrolyte oxidation suppression. Finally, accelerating rate calorimetry (ARC) testing revealed substantially lower self-heating rates from 50 to 300 °C for F4DEE-containing cells compared to DEE-containing ones, highlighting enhanced safety performance.

## Materials and Methods

***Electrode and electrolyte preparation.***—NCMFNZO/HC dry pouch cells (210 mAh, Lifun Technology, Zhuzhou, Hunan) were sourced, with specifications detailed previously.[16,17] The cathode and anode active materials have loadings of 16 mg $cm^{-2}$ and 9.47 mg $cm^{-2}$, respectively, on aluminum foil current collectors with an active electrode area of 99.58 $cm^2$. For symmetric cell fabrication, pouch cells were disassembled in an Ar-filled glovebox, and the jelly roll was unrolled to separate cathode and anode. Single-side-coated cathodes were prepared by removing material from one side of the current collector using N-methyl pyrrolidone (NMP). Cathode and anode samples (0.95 $cm^2$) were punched for coin cells. Symmetric CR2032 coin cells were assembled with a polypropylene blown microfiber (BMF) separator and 150 µl of electrolyte. Electrolytes were formulated at 1 m sodium bis(fluorosulfonyl)imide (NaFSI, >99.0%, CapChem) in 1,2-diethoxyethane (DEE, >99.5%, $H_2O$ <20 ppm, Feon Energy Inc.) or fluorinated ether (F4DEE, >99.5%, $H_2O$ <20 ppm, Feon Energy Inc.), with 2 wt% fluoroethylene carbonate (FEC, $H_2O$ <20 ppm, CapChem) added as an additive.

In the electrolytes, the self-diffusion coefficients of $^{19}F$ and $^{23}Na$ ($D_F$ and $D_{Na}$, respectively) were measured on a Varian/Agilent 300 MHz WB NMR spectrometer equipped with a DOTY z-gradient probe, with Larmor frequencies at 282.4 MHz and 79.4 MHz for $^{19}F$ and $^{23}Na$, respectively. The self-diffusion coefficient of $^{19}F$ was measured at 25 °C and the self-diffusion coefficient of $^{23}Na$ was measured at 60 °C. A spin-echo sequence was used with gradient pulse durations ( ) of 2 ms, diffusion delay durations (Δ) of 8–30 ms, and gradient field strength (g) varied from 3 to 900 G $cm^{-1}$ across 4 to 256 transient scans as needed for improved S/N ratio. The self-diffusion coefficient for $^{23}Na$ in the sample with F4DEE was unobtainable due to relaxation times faster than the timescale of the diffusion measurement.

The self-diffusion coefficients are related to their viscosities by the Stokes-Einstein-Sutherland equation:

$$D = \frac{k_B T}{6\pi\eta r} \quad [1]$$

where $k_B$ is the Boltzmann constant, $T$ is absolute temperature, $\eta$ is viscosity, and $r$ is the Stokes radius of the spherical particle. By comparing the ratios of the sample viscosities and the self-diffusion coefficients of $^{19}F$ corresponding to $FSI^-$ of 1 m NaFSI in DEE + 2% FEC and 1 m NaFSI in F4DEE + 2% FEC at 25 °C using the relation,

$$\frac{D_{F4DEE}}{D_{DEE}} \propto \frac{\eta_{DEE}}{\eta_{F4DEE}} \quad [2]$$

the effect of the increase in viscosity on diffusion can be observed (Table I). In addition, the ratio of the conductivities is compared to the inverse ratio of the viscosity.

***Electrochemical measurements.***—All NCMFNZO/HC dry pouch cells were filled with 1 g of electrolyte and sealed using a vacuum sealer (MSK-115A-111, MTI Corp.) at −85 kPa, 165 °C sealing bar temperature, for 5 s in an Ar-filled glovebox (<0.01 ppm $O_2/H_2O$). During formation, cells were placed in temperature-controlled chambers (Neware, Shenzhen) at 40 ± 0.1 °C, rested for 3 h, charged to 4 V at C/20, and discharged to 3.1 V at C/20 for degassing. Long-term cycling was performed between 1.5 V and 4.0 V at 25 °C and 40 °C using constant current constant voltage (CCCV) mode at C/5 with a C/20 cut-off current, including a C/20 check-up cycle every 50 cycles to study capacity loss due to Na inventory loss. During storage testing, cells underwent two C/20 cycles at 40 °C, followed by 500 h open-circuit storage at 4.0 V. Electrochemical impedance spectroscopy (EIS) testing was performed using a BioLogic VMP3. Ten data points were collected per decade from 100 kHz to 100 mHz with a 10 mV amplitude at 25 °C.

***Cells and materials characterization.***—Gas generated in pouch cells during formation, and storage was quantified using Archimedes' principle, as reported by Aiken et al.[18] Soft X-ray absorption measurements were performed at the Stanford Synchrotron Radiation Lightsource (SSRL), beamline 8-2, with X-ray incidence set to 55° (approximate magic angle). All samples at different charged or discharged states were recovered from a cell in an Ar-filled glove box. The electrodes were subsequently rinsed with dimethyl carbonate (DMC) and dried inside the glove box. A small portion of each electrode was mounted on an aluminum stick and sealed under an Ar atmosphere. The sealed samples were then transferred through a vacuum chamber and mounted for soft XAS measurements. For each sample, at least two scans were collected. Ni L-edge spectra were collected using a 1000 lines $mm^{-1}$ grating with 60 µm × 60 µm entrance slits, yielding an energy resolution of 0.35 eV. The beam spot at the sample was approximately 1 × 1 $mm^2$ and the incident flux was on the order of 1 × $10^{10}$ photons $s^{-1}$; under these conditions no beam damage was observed. Spectra were acquired in both total electron yield (TEY) and total fluorescence yield (TFY) modes: TEY was measured as the drain current amplified by a Keithley picoammeter, and TFY was detected with a silicon diode (IRD AXUV-1000). The incident flux ($i_0$) was monitored upstream using a nickel mesh with a Au sputtered film. Electrode specimens were mounted on carbon tape and attached to aluminum sample holders. All spectra were processed and normalized using PyMCA.

Energy dispersive X-ray fluorescence (EDXRF) measurements were conducted using a Rigaku NEX DE benchtop spectrometer with a 10 mm spot size and Rh-target X-ray source (Tokyo, Japan). Measurement of Na-K characteristic X-rays in the low-Z range used no filter, 6.5 kV tube voltage, 376 µA tube current, and 100 s measurement time. Measurement of Mn-K , Fe-K , and Ni-K characteristic X-rays in the mid-Z range used a C filter, 35 kV tube voltage, 274 µA tube current, and 100 s measurement duration. Samples were extracted from pouch cells before and after cycling and storage tests, then gently dried in a vacuum chamber (<20 mbar). Additional confirmation of the resolution of EDXRF for small quantities of transition metals on carbon electrodes was obtained using graphite electrodes with 10 nm Au sputtered deposits. These control samples were accurately confirmed to have a 20 µg $cm^{-2}$ loading.

During accelerating rate calorimetry (ARC) testing, two pouch cells were wrapped around one thermocouple of an accelerating rate calorimeter (EV+, Thermal Hazard Technology).[2] ARC testing was performed under adiabatic conditions. Self-heating was recognized

**Table I. A summary of transport properties of selected electrolytes.**

| Electrolyte | Conductivity, σ (mS $cm^{-1}$) | Viscosity, $\eta$ (Cp) | $D_{23\_Na}$ ($m^2$ $s^{-1}$) | $D_{19\_F}$ ($m^2$ $s^{-1}$) |
|---|---|---|---|---|
| 1 m NaFSI in DEE + 2% FEC | 3.27 | 1.620 | 2.47 * $10^{-10}$ ± 10% | 1.59 × $10^{-10}$ |
| 1 m NaFSI in F4DEE + 2% FEC | 2.39 | 7.077 | N/A | 8.82 × $10^{-11}$ |
| $\frac{D_{F4DEE}}{D_{DEE}}$ or $\frac{\eta_{DEE}}{\eta_{F4DEE}}$ or $\frac{\sigma_{F4DEE}}{\sigma_{DEE}}$ | 0.731 | 0.229 | N/A | 0.555 |

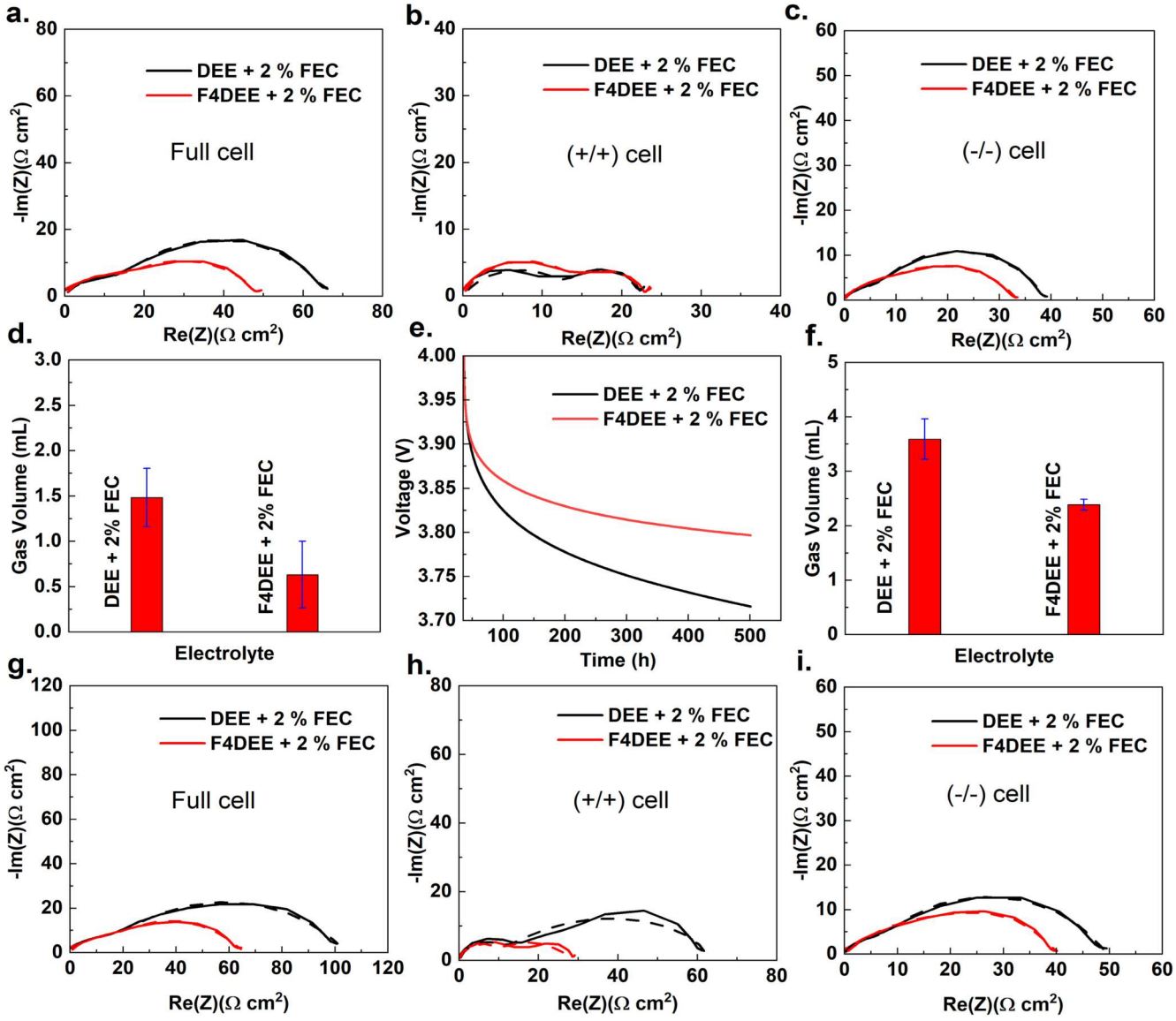


**Figure 1.** Assessment of the effects of electrolyte composition on the formation and open circuit storage process of NCMFNZO/HC pouch cells. (a) Nyquist plot of the area specific impedance of NCMFNZO/HC pouch cells at 3.1 V after cell formation. Nyquist plot of the area specific impedance of (b) NCMFNZO/NCMFNZO symmetric cells and (c) HC/HC symmetric cells reconstructed from NCMFNZO/HC pouch cells at 3.1 V after formation. (d) Gas volume of pouch cells during formation. (e) Voltage vs time, (f) gas volume evolution, and (g) Nyquist plot of the area specific impedance of NCMFNZO/HC pouch cells at 3.1 V after 500 h open circuit storage at 4.0 V and 40 °C. Nyquist plot of the area specific impedance of (h) NCMFNZO/NCMFNZO symmetric cells and (i) HC/HC symmetric cells reconstructed from NCMFNZO/HC pouch cells at 3.1 V after storage as shown in (e). All impedance measurements were performed at 25 °C. Each spectrum is the average results of two cells measurement.

when the sample's self-heating rate (SHR) exceeded 0.02 °C $min^{-1}$. All the testing was performed within the temperature range of 50 °C to 315 °C, with a heating step of 5.0 °C/step. Experiments were programmed to terminate automatically if the temperature exceeded 350 °C or the SHR surpassed 10 °C $min^{-1}$ to ensure safety and equipment integrity.

After the formation cycle, cells designated for isothermal microcalorimetry underwent "conditioning" cycles to ensure a stable solid electrolyte interphase (SEI) layer.[19] Cells were cycled ten times between 1.5 V and 4.0 V at C/5 using Keithley 2602B source-measure units at 40 ± 0.1 °C in Cyclikal CT1601 temperature chambers. Subsequently, cells were placed in a TAM IV thermostat with 20 ml microcalorimeters (TA Instruments, temperature stability ±0.0001 °C, accuracy ±1 μW, precision ±1 nW) set to a constant 40.0000 °C. For in-calorimeter cycling, cells were connected to Keithley 2602B units and cycled at C/10 for five cycles between 1.5 V and 4.0 V, followed by five cycles at C/120 between 3.6 V and 4.0 V. Duplicate cells with identical electrolyte were assembled to ensure repeatability of isothermal microcalorimetry results. Calorimeter wiring for cell cycling and calibration were as described by Krause et al.[20]

## Results and Discussion

Utilizing DEE (non-fluorinated ether) and F4DEE (fluorinated ether) solvents (Fig. S1), we observed that fluorination slightly reduces transport properties, including ionic conductivity and viscosity (Table I). Interestingly, 19 F-NMR measurements of the $FSI^-$ anion diffusion coefficient at room temperature show that diffusion does not scale with viscosity (Table I), suggesting different ion-transport mechanisms between the two electrolytes, likely arising from different solvation structures. The impact of this fluorination on electrochemical performance was evaluated in NCMFNZO/HC pouch cells during formation and high-voltage, high-temperature open-circuit storage (Fig. 1). Fluoroethylene carbonate (FEC) was

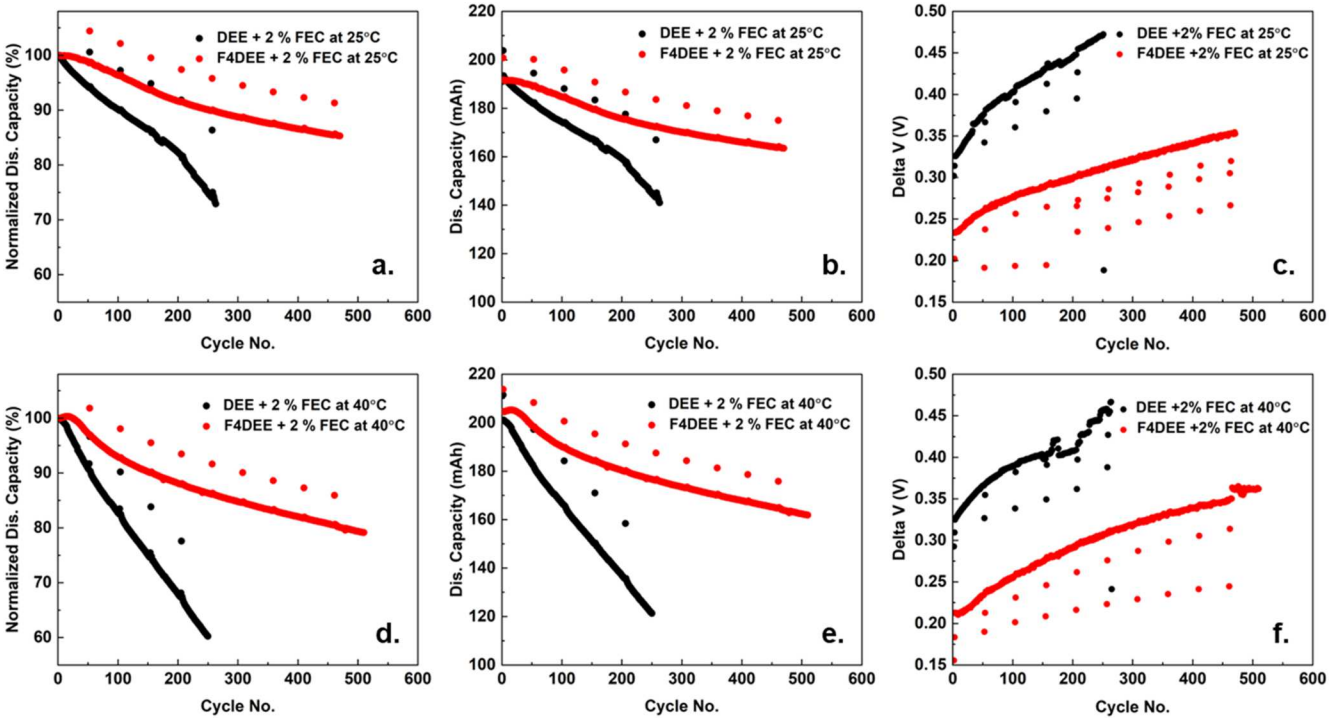


**Figure 2.** Evaluation of the effects of electrolyte compositions on the long-term cycling performance of NCMFNZO/HC pouch cells. (a) normalized discharge capacity, (b) discharge capacity, (c) delta V vs cycling No. during long-term cycling between 1.5 and 4.0 V at 25 °C with a rate of C/5 in CCCV mode with a C/20 cut-off current. (d) Normalized discharge capacity, (e) discharge capacity, (f) delta V vs cycling No. during long-term cycling between 1.5 and 4.0 V at 40 °C with a rate of C/5 in CCCV mode with a C/20 cut-off current. C/20 was performed every 50 cycles.

added to both solvent systems to ensure HC anode passivation and enable a fair solvent comparison. DEE cannot form a stable SEI on its own: cells without FEC produce excessive gas during formation and fail, whereas F4DEE has intrinsic film-forming capabilities; investigation of F4DEE's standalone interphase behavior is the subject of a separate study.[21] Notably, F4DEE-containing cells exhibited lower impedance post-formation (Fig. 1a). To understand the source of this impedance difference, symmetric cells were constructed and tested, revealing comparable impedance at the NCMFNZO cathode (Fig. 1b) but significantly reduced impedance at the HC anode (Fig. 1c) in F4DEE-containing cells. Additionally, DEE-containing cells generated more gas during formation compared to F4DEE-containing cells (Fig. 1d).

After formation, cells underwent two cycles at C/20, followed by 500 h of open-circuit storage at 4.0 V and 40 °C. F4DEE-containing cells showed minimal voltage drop (Fig. 1e) and reduced gas generation during storage (Fig. 1f), indicating superior resistance to electrolyte oxidation at high voltage. Post-storage Nyquist plots, measured at 3.1 V and 25 °C (Fig. 1g), confirmed lower impedance growth in F4DEE-containing cells. EIS tests of symmetric cells (Figs. 1h–1i) further demonstrated that F4DEE suppresses impedance growth at both the NCMFNZO cathode (Fig. 1h and HC anode (Fig. 1i) compared to DEE-containing cells. In addition, slightly higher Ni and Mn dissolution and redeposition on the HC anode was observed via EDXRF for DEE-containing cells compared with F4DEE-containing cells after storage (Fig. S2).

To study the effect of ether fluorination on the cycling lifetime of SIBs, NCMFNZO/HC pouch cells were cycled at a C/5 rate in CCCV mode with a C/20 cut-off current, between 1.5 V and 4.0 V, at both 25 °C (Figs. 2a–2c) and 40 °C (Figs. 2d–2f), respectively. Periodic slow rate (i.e. C/20) cycling check-up cycles were performed every 50 cycles to evaluate Na inventory loss. Fluorination of the DEE solvent (i.e. F4DEE) extends capacity retention in NCMFNZO/HC pouch cells compared to the control at both 25 °C (Figs. 2a–2b) and 40 °C (Figs. 2d–2e), achieving 85% retention after 500 cycles at 25 °C (Fig. 2a) and 80% at 40 °C (Fig. 2d). The mitigation of Na inventory loss was also evidenced by the check-up cycling data. This improvement correlates with reduced transition-metal dissolution (i.e. Ni, Fe, Mn) at the HC anode in F4DEE-containing cells compared with DEE-containing cells (Fig. S2). Delta V, defined as the difference between average charge and discharge voltages, suggests polarization growth during cycling (Figs. 2c, 2f); F4DEE shows only marginal improvement in controlling polarization at both temperatures. It is worth noting that the F4DEE-containing electrolyte shows worse transport properties than the DEE-containing electrolyte at 25 °C (Table I), which likely causes the small initial capacity difference observed at both C/5 and C/20 in Fig. 2b. At C/5 and C/20 this effect is minor, but determining the rate at which the capacity reduction becomes significant at 25 °C is important for power-cell design and warrants further study. Unfortunately, F4DEE does not suppress Na plating on the HC anode during cycling (Fig. S3). No major morphological differences were observed for the NCMFNZO cathode or HC anode after cycling in the two electrolytes (Fig. S4).

To elucidate the extended cycle life of SIBs with F4DEE compared to DEE, isothermal microcalorimetry coupled with ultra-high precision coulometry (UHPC) was conducted (Fig. 3). Duplicate cells for each electrolyte composition ensured repeatability. Post-formation, cells underwent 10 conditioning cycles (C/5, 1.5–4.0 V, 40 °C) before being transferred to an isothermal microcalorimeter with a bath temperature of 40 °C. Two sequential testing protocols were implemented to systematically study heat flow differences between the two electrolytes, revealing the mechanisms behind F4DEE's ability to enhance cell lifetime. In the first protocol, cells were cycled five times at C/10 between 1.5 and 4.0 V, with simultaneous heat flow measurements to capture full voltage range thermal behavior. F4DEE-containing cells exhibited better discharge capacity retention (Fig. 3a) and a coulombic efficiency (CE) of 0.998 (Fig. 3b), compared to 0.994 for DEE-containing cells, which showed poorer discharge capacity retention. F4DEE-containing cells also showed a lower rate of charge endpoint slippage (Fig. 3c), indicating better suppression of electrolyte oxidation, and

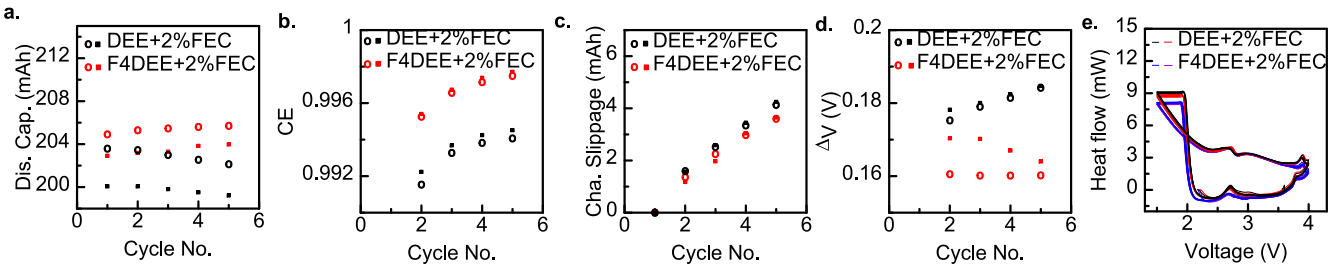


**Figure 3.** Evaluation of the effects of electrolyte compositions on the heat flow of NCMFNZO/HC pouch cells during UHPC cycling. (a) Discharge capacity, (b) CE, (c) charge endpoint slippage, and (d) delta V vs cycling number of NCMFNZO/HC pouch cells during UHPC cycling at 40 °C and C/10 between 1.5 and 4.0 V. (e) Heat flow vs voltage of NCMFNZO/HC pouch cells during UHPC cycling (a-d).

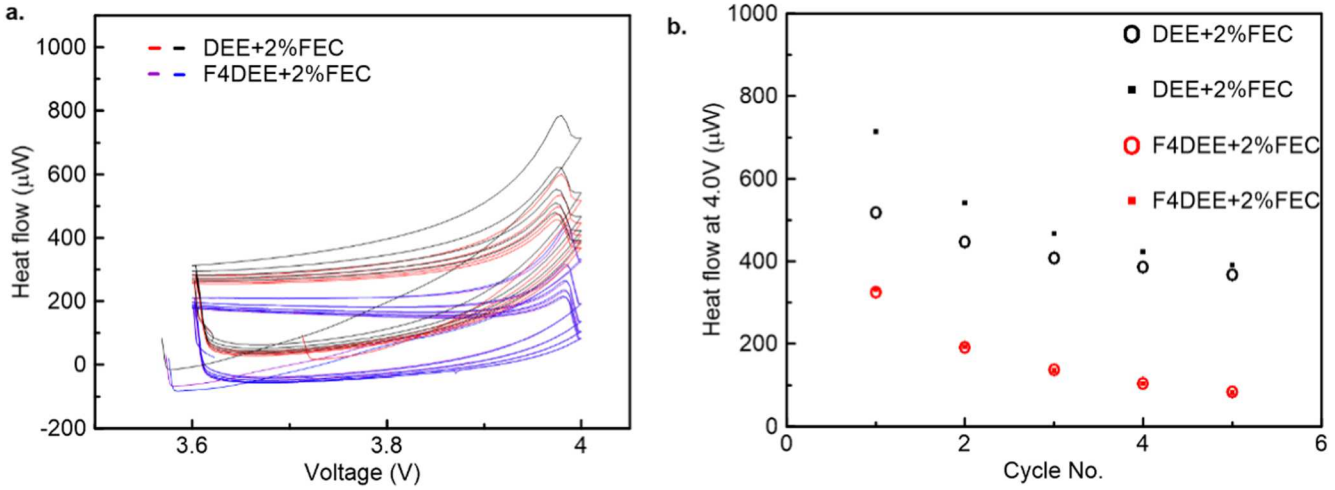


**Figure 4.** Evaluation of the effects of electrolyte compositions on the heat flow of NCMFNZO/HC pouch cells during UHPC cycling between 3.6 and 4.0 V at C/120 and 40 °C. (a) Heat flow vs voltage; (b) measured heat flow at 4.0 V.

reduced delta V growth, suggesting lower polarization growth (Fig. 3d). Heat flow results revealed a combination of contributions from entropy changes, polarization, and parasitic reactions.[22] Typical reversible thermal features (Figs. S5, 3e) likely tied to cathode phase transitions or highly sodiated states were observed with no significant changes after cycling. Notably, F4DEE-containing cells generated lower thermal power at high voltages (3.6–4.0 V) and at low voltages (1.5–3.0 V), suggesting fewer parasitic electrolyte-cathode reactions as well as less entropic and polarization heating potentially due to a more robust electrode-electrolyte interphase, respectively (Fig. 3e).

In the subsequent second protocol, focusing on high-voltage (3.6–4.0 V) behavior, cells were cycled five times at C/120 with concurrent heat flow monitoring. F4DEE-containing cells maintained better capacity retention (Fig. S6a) but both electrolytes showed lower CE ( 0.96 for F4DEE-containing cells vs 0.92 for DEE-containing cells, Fig. S6b) than in full-range cycling, indicating faster degradation due to pronounced electrolyte oxidation. This is also evidenced by increased charge endpoint slippage (Fig. S6c). F4DEE-containing cells still outperform DEE-containing cells in controlling electrolyte oxidation. Greater voltage hysteresis was observed in DEE-containing cells (Fig. S6d). Heat flow at C/120 was lower than at C/10 due to reduced current, but F4DEE-containing cells consistently produced less thermal power across 3.6–4.0 V during each cycle (Fig. 4a), with 80% lower thermal power than DEE cells at 4.0 V on cycle 5 (Fig. 4b), confirming a significant reduction in parasitic reactions with F4DEE.

Given that F4DEE-containing cells demonstrate an extended cycle life compared to DEE-containing cells (Fig. 2), attributed to their superior suppression of electrolyte oxidation at high voltage as evidenced during open-circuit storage (Fig. 1e) and isothermal microcalorimetry testing (Fig. 3), the CEI was characterized using ensemble-averaged, surface-sensitive soft XAS (Fig. 5). Fluorescence yield (FY) and total electron yield (TEY) modes probed subsurface (50 nm) and surface (10 nm) chemical environments, respectively. Transition metal oxidation states were studied using the intensity ratio of high- to low-energy shoulders in the L3-edge spectra, where a higher ratio suggests higher oxidation states.[23,24] Comparing FY and TEY spectra showed depth-dependent chemical changes affected by electrolyte composition during long-term cycling, with a focus on Ni, Fe, and Mn. As shown in Fig. 5, F4DEE-containing samples exhibited higher average Ni and Mn oxidation states in both TEY and FY modes, with comparable Fe oxidation states across both modes. These findings indicate that DEE-containing samples undergo Ni and Mn reduction at both surface and subsurface levels due to electrolyte oxidation. In contrast, the CEI formed with F4DEE shows enhanced stability, effectively suppressing electrolyte oxidation and mitigating Ni and Mn reduction at the surface.

ARC was finally conducted to evaluate the impact of polyfluorination of the terminal ether alkyls on the thermal stability of SIB pouch cells (Fig. 6). Duplicate tests were performed for repeatability; each pouch cell contained 1 g of electrolyte to ensure consistent electrolyte mass across cells. Compared to DEE-containing cells, the F4DEE-containing cells exhibited enhanced thermal stability, with a delayed exothermic onset temperature of 125 °C vs 75 °C. Additionally, the self-heating rate (SHR) of F4DEE-containing cells was much lower across the tested temperature range up to 300 °C,

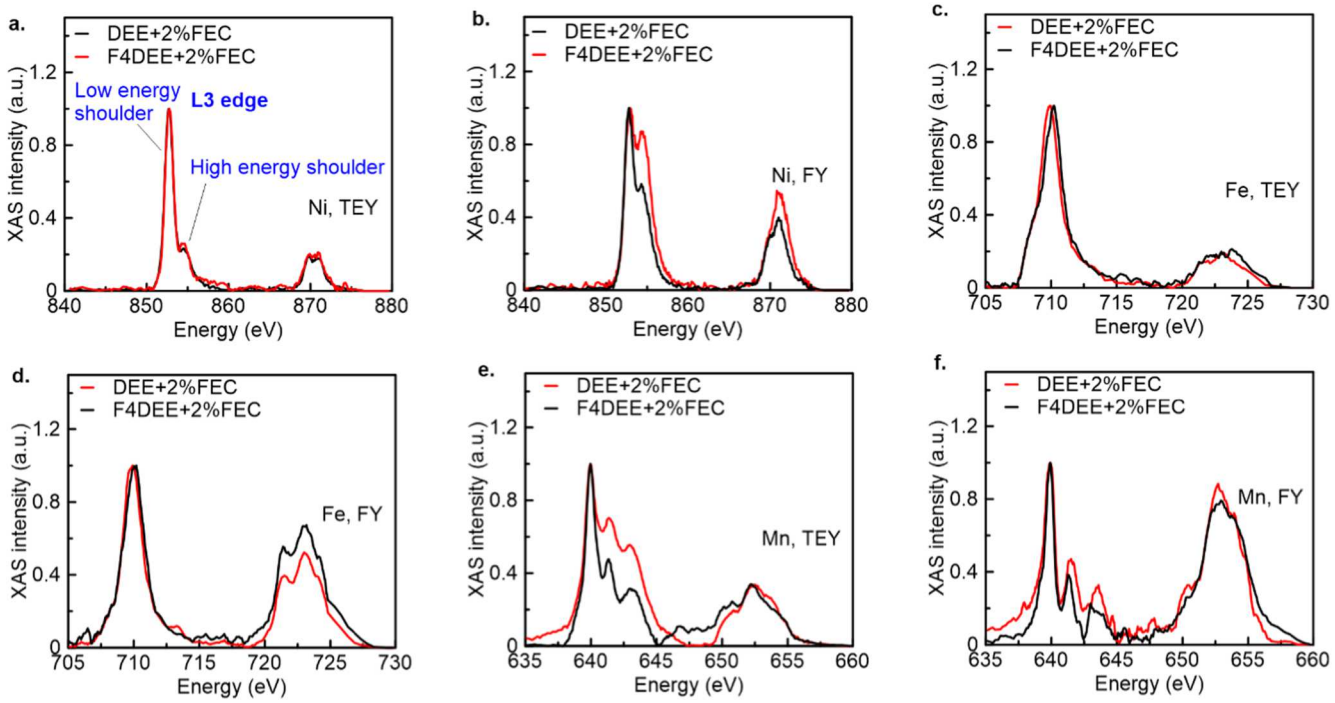


**Figure 5.** Evaluation of CEI of NCMFNZO after long term cycling at 40 °C using soft XAS spectroscopy. (a–b) Ni L-edge for NCMFNZO cathode in (a) TEY and (b) FY mode. (c–d) Fe L-edge for NCMFNZO cathode in (d) TEY and (e) FY mode. (e–f) Fe L-edge for NCMFNZO cathode in (e) TEY and (f) FY mode.

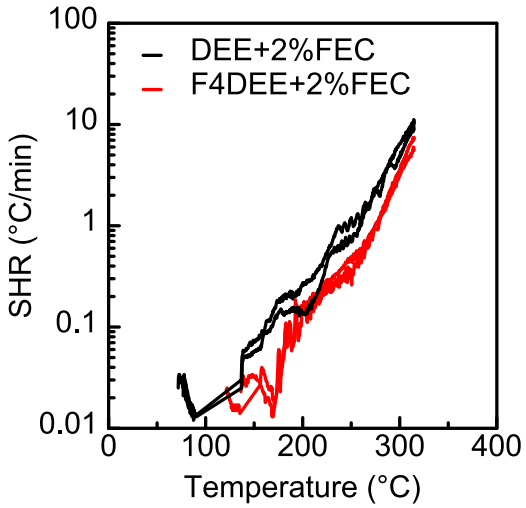


**Figure 6.** SHR vs temperature for NCMFNZO/HC pouch cells with different electrolytes at 4.0 V after formation. Each ARC testing includes two pouch cells.

indicating improved safety through fluorinated ether solvents in SIBs. Nail-penetration testing is worth pursuing to assess the effect of F4DEE on cell safety under an additional abuse condition.[25]

## Conclusions

In summary, we systematically compared non-fluorinated DEE and the fluorinated F4DEE as sole electrolyte solvents in 210 mAh NCMFNZO/HC pouch cells. Although fluorination slightly reduced bulk transport properties at room temperature, including ionic conductivity and viscosity, F4DEE yielded clear electrochemical and safety advantages. Cells with F4DEE exhibited lower impedance at both cathode and anode, with reduced gas evolution and voltage decay during high-voltage (4.0 V) and high-temperature (40 °C) storage. Long-term cycling demonstrated extended cell lifetime, with approximately 85% capacity retention after 500 cycles at 25 °C, and around 80% after 500 cycles at 40 °C. These improvements are attributed to less transition metal dissolution and F4DEE's ability to suppress electrolyte oxidation, as evidenced by UHPC cycling showing less rate of charge endpoint slippage and isothermal calorimetry indicating reduced parasitic heat flow between 3.6 and 4.0 V. Soft X-ray absorption spectroscopy of the CEI confirmed that fluorination helps stabilize Ni and Mn oxidation states, supporting a mechanistic role in suppressing electrolyte oxidation. ARC testing further demonstrated enhanced thermal stability with F4DEE, highlighting its safety benefits.

Overall, molecular fluorination of ether solvents offers a promising strategy to improve both the longevity and safety of SIBs. Remaining challenges include modest transport tradeoffs and persistent Na plating, emphasizing the need for further solvent and additive optimization. Future work should focus on tuning fluorinated solvent structures, exploring complementary film-forming additives, and conducting operando or atomistic studies to better suppress Na plating and extend cell lifetime for practical applications.

## Acknowledgments

Dr L.M. acknowledges the support by the US National Science Foundation Award No. 2301719. Dr Mu acknowledges the support from the ASU startup funds. The authors also acknowledge the use of Beamline 8–2 with assistance from Dr. Dennis Nordlund at the Stanford Synchrotron Radiation Light source, SLAC National Accelerator Laboratory, which was supported by the U.S. Department of Energy, Office of Science, Office of Basic Energy Sciences under Contract no. DE-AC02–76SF00515.

## ORCID

Rishivandhiga Jayakumar https://orcid.org/0009-0004-1501-2597
Benjamin Cousineau https://orcid.org/0000-0003-1603-008X
Vincent L. Chevrier https://orcid.org/0000-0002-8725-0787
Chanmonirath (Michael) Chak https://orcid.org/0009-0004-6750-4251
Vadim Shipitsyn https://orcid.org/0009-0008-6521-0216
Allen Zheng https://orcid.org/0000-0001-8895-8579
Yuwei Zhu https://orcid.org/0009-0001-2145-8067

Glenn Pastel https://orcid.org/0000-0002-0212-1397
Zhiao Yu https://orcid.org/0000-0001-8746-1640
Linqin Mu https://orcid.org/0000-0003-4421-4820
Steve G. Greenbaum https://orcid.org/0000-0001-5497-5274
Lin Ma https://orcid.org/0000-0003-1183-1347

## References

1. Y. Gao, H. Zhang, J. Peng, L. Li, Y. Xiao, L. Li, Y. Liu, Y. Qiao, and S. Chou, "A 30-year overview of sodium-ion batteries." *Carbon Energy*, **6**, e464 (2024).
2. C. (M.) Chak, R. Jayakumar, V. Shipitsyn, E. Bass, R. McCloskey, W. Zuo, P. M. L. Le, J. Xu, and L. Ma, "Unveiling the thermal stability of sodium ion pouch cells using accelerating rate calorimetry." *J. Electrochem. Soc.*, **171**, 070512 (2024).
3. A. Yao, S. M. Benson, and W. C. Chueh, "Critically assessing sodium-ion technology roadmaps and scenarios for techno-economic competitiveness against lithium-ion batteries." *Nat. Energy*, **10**, 404 (2025).
4. J. Chen, G. Adit, L. Li, Y. Zhang, D. H. C. Chua, and P. S. Lee, "Optimization strategies toward functional sodium-ion batteries." *ENERGY Environ. Mater.*, **6**, e12633 (2023).
5. Y. S. Meng, V. Srinivasan, and K. Xu, "Designing better electrolytes." *Science*, **378**, eabq3750 (2022).
6. K. Xu, "Electrolytes and interphases in Li-Ion batteries and beyond." *Chem. Rev.*, **114**, 11503 (2014).
7. Y. Li, F. Wu, Y. Li, M. Liu, X. Feng, Y. Bai, and C. Wu, "Ether-based electrolytes for sodium ion batteries." *Chem. Soc. Rev.*, **51**, 4484 (2022).
8. F. Cheng, J. Hu, W. Zhang, B. Guo, P. Yu, X. Sun, and J. Peng, "Reviving ether-based electrolytes for sodium-ion batteries." *Energy Environ. Sci.*, **18**, 6874 (2025).
9. S. Li, M. Jin, X. Song, S. Xu, Q. Dou, J. Zhu, and X. Yan, "Revisiting ether electrolytes for high-voltage sodium-ion batteries." *Energy Storage Mater.*, **73**, 103815 (2024).
10. Z. Yu et al., "Rational solvent molecule tuning for high-performance lithium metal battery electrolytes." *Nat. Energy*, **7**, 94 (2022).
11. Y. Lin et al., "Impact of the fluorination degree of ether-based electrolyte solvents on Li-metal battery performance." *J. Mater. Chem. A*, **12**, 2986 (2024).
12. A. A. Hizbullin, I. V. Kutovaya, G. A. Kirakosyan, D. A. Cheshkov, D. N. Govorov, D. A. Aksyonov, V. A. Nikitina, S. S. Fedotov, and O. I. Shmatova, "A fluorinated ether electrolyte for high-performance lithium metal batteries: compatibility with $LiPF_6$ and long-term cycling." *J. Power Sources*, **630**, 236086 (2025).
13. Y. Xue, Y. Wang, H. Zhang, W. Kong, Y. Zhou, B. Kang, Z. Huang, and H. Xiang, "Molecular design of mono-fluorinated ether-based electrolyte for all-climate lithium-ion batteries and lithium-metal batteries." *Angew. Chem.*, **137**, e202414201 (2025).
14. E. Zhang et al., "Monofluorinated acetal electrolyte for high-performance lithium metal batteries." *Proc. Natl Acad. Sci.*, **122**, e2418623122 (2025).
15. Y. Zhao, T. Zhou, M. Mensi, J. W. Choi, and A. Coskun, "Electrolyte engineering via ether solvent fluorination for developing stable non-aqueous lithium metal batteries." *Nat. Commun.*, **14**, 299 (2023).
16. V. Shipitsyn, R. Jayakumar, W. Zuo, W. Yin, E. Huber, and L. Ma, "The impact of fluoroethylene carbonate additive on charged sodium ion electrodes/electrolyte reactivity studied using accelerating rate calorimetry." *J. Electrochem. Soc.*, **170**, 110501 (2023).
17. R. Jayakumar et al., "Weakly solvating ester electrolyte for high voltage sodium-ion batteries." *Nano Energy*, **128**, 109969 (2024).
18. C. P. Aiken, J. Xia, D. Y. Wang, D. A. Stevens, S. Trussler, and J. R. Dahn, "An Apparatus for the study of In Situ gas evolution in Li-ion pouch cells." *J. Electrochem. Soc.*, **161**, A1548 (2014).
19. S. L. Glazier, L. E. Downie, J. Xia, A. J. Louli, and J. R. Dahn, "Effects of fluorinated carbonate solvent blends on high voltage parasitic reactions in lithium ion cells using OCV isothermal microcalorimetry." *J. Electrochem. Soc.*, **163**, A2131 (2016).
20. L. J. Krause, L. D. Jensen, and V. L. Chevrier, "Measurement of Li-Ion battery electrolyte stability by electrochemical calorimetry." *J. Electrochem. Soc.*, **164**, A889 (2017).
21. R. Jayakumar and L. Ma, "Ethylene sulfate-enabled stable interphases in fluorinated ether electrolytes for high-performance sodium-ion batteries." *J. Power Sources*, **662**, 238753 (2026).
22. L. E. Downie, S. R. Hyatt, A. T. B. Wright, and J. R. Dahn, "Determination of the time dependent parasitic heat flow in lithium ion cells using isothermal micro-calorimetry." *J. Phys. Chem. C*, **118**, 29533 (2014).
23. L. Mu et al., "Deciphering the cathode–electrolyte interfacial chemistry in sodium layered cathode materials." *Adv. Energy Mater.*, **8**, 1801975 (2018).
24. L. Mu et al., "Revealing the chemical and structural complexity of electrochemical ion exchange in layered oxide materials." *J. Am. Chem. Soc.*, **146**, 26916 (2024).
25. X. Gao, Y. Jia, W. Lu, Q. Wu, X. Huang, and J. Xu, "Mechanistic understanding of reproducibility in nail penetration tests." *Cell Rep. Phys. Sci.*, **4**, 101542 (2023).